Impedance analysis of the AC behaviour of a $Au/Pb_2CrO_5/SnO_2$ thin-film device

1997 J. Phys.: Condens. Matter 9 3609

(http://iopscience.iop.org/0953-8984/9/17/010)

J. Phys.: Condens. Matter **9** (1997) 3609–3623. Printed in the UK PII: S0953-8984(97)75347-5

Impedance analysis of the AC behaviour of a $Au/Pb_2CrO_5/SnO_2$ thin-film device

Kohji Toda†, M M Abdul-Gader‡ and Masahiko Okada†

† Department of Electronic Engineering, National Defense Academy, Hashirimizu, Yokosuka 239, Japan

‡ Department of Physics, University of Jordan, Amman, Jordan

Received 12 June 1996, in final form 2 January 1997

Abstract. Impedance and phase measurements on a $Au/Pb_2CrO_5/SnO_2$ sandwiched-structure thin-film device 0.8 μm thick were carried out at room temperature as a function of frequency in the range 0.1 Hz–1.0 MHz under dark and visible-light environments (0–64.8 mW cm^{-2}). A thorough impedance analysis was carried out using two types of equivalent-circuit model to explain the observed AC behaviour. One of these models utilizes the classical concept of interfacial space-charge polarization based on the Maxwell–Wagner two-layer capacitor system, whereas the other takes into consideration the physical meaning of a $Au/Pb_2CrO_5/SnO_2$ optoelectronic device. The latter model has been invoked to calculate the individual electrical, photoelectric and dielectric parameters of the Pb_2CrO_5. The results of such an analysis enable us to deduce a value for the room-temperature volume dark resistivity ρ_d of the Pb_2CrO_5 material equal to 2.6×10^9 Ω cm. Furthermore, these results confirm that the photoconduction phenomenon in Pb_2CrO_5 is due to semiconductivity with the photoconductivity σ_{phot} varying with light intensity F according to the generally accepted experimental power law of the form $\sigma_{phot} \propto F^m$, with $m = 0.7(\pm 5\%)$. The relative dielectric constant κ of this semi-insulating material has been found, for the first time, to have a value of 14.9, irrespective of the illumination level. On the other hand, the electrical, photoelectric and dielectric properties associated with the Au–Pb_2CrO_5 contact, which is probably responsible for the low-frequency dispersion in the device, were found to have a large influence on its overall AC characteristics and this has been attributed to interfacial space-charge effects which seem to be enhanced by illumination.

1. Introduction

The electrical properties of the surface and interfacial layers of dielectric specimens are often different from those of the bulk of the material. These differences are often attributable to contact effects between the electrodes and the specimen [1–18]. The phenomenon is important both from the view-point of the measurement and interpretation of the electrical and dielectric properties of dielectrics and from the view-point of the application of these materials in engineering practice. For some applications, it is not only the bulk electrical properties of the dielectric material which are significant, but also the properties of the surface and interfacial layers where contacts are made from metallic components. Knowledge of contact and interfacial effects enables a combination of electrodes and dielectric to be chosen such that the results of measurements of the electrical properties are only a little different from the internal properties of the dielectric.

For thin dielectric and semiconductor specimens, contact effects have a greater influence on the properties of the combination of metallic electrode–dielectric–metallic electrode

0953-8984/97/173609+15$19.50

than they have for thick specimens, and the difference between measured properties and internal properties becomes correspondingly more significant. These effects have become of practical significance as electrical or microelectronic devices usually incorporate integrated-circuit combinations such as metal–insulator–metal, metal–semiconductor–metal and similar thin-film arrangements [4–19]. In general, these thin-film systems usually involve inhomogeneous parts brought about by structural changes and/or by the creation of surface layers caused by the absorption of atoms, ions or electrons from the surroundings. Thus, electrode and interfacial space-charge effects become important and operative in such systems and can sometimes lead to electrical and dielectric performance of these structures that will be dependent on the applied external agents such as DC-biasing conditions, specimen thickness, illumination, and the frequency or amplitude of the AC signal used. This often renders reliable measurements of electrical and/or dielectric properties of the interior of the specimen difficult to obtain and makes their interpretations more complex.

A powerful customary experimental method which has been invoked to investigate the AC behaviour of such electrical-circuit combinations is the use of AC-impedance spectroscopy techniques [10–14, 20–25]. The results of these AC methods are often analysed and interpreted by adopting a proper equivalent-circuit model as such an approach usually enables one to separate the influence of the electrode and interfacial effects from the inherent bulk properties of the device under investigation. In general, one cannot find a universal type of equivalent-circuit model that describes the electrical AC behaviour of all dielectric systems, and even an individual one can only be assumed to be a simplified representation and/or to achieve a specific interpretation of the experimental results. The electrical-circuit models based on the conventional Maxwell–Wagner (MW) two-layer capacitor system [3–6] or those considering the physical meaning of an electrical or optoelectronic device [10–14,21–25] are sometimes applicable and informative. We have adopted the MW model as well as a specific physical model of the latter type to describe the structure of our device and its overall electrical and dielectric properties as will be discussed later.

One of the important and attractive materials that has recently received considerable attention for use in photoconductors and microelectronic optical devices in the ultraviolet and visible regions of the spectrum is Pb_2CrO_5 [15–19, 26–31]. Pb_2CrO_5, in the system PbO–chromium oxide [32, 33], is described as a dielectric material because of its centrosymmetry in the C2/m space group. This material has been found to have a wide band-gap energy E_g($\sim$ 2.1–2.3 eV), a large absorption coefficient $\alpha \sim 10^4$–10^5 cm^{-1} and a high photoresponse speed in this spectral region. Thin films of this material were considered to be more informative and suitable for integration of photosensor elements than specimens in the ceramic form. Structural, optical and electrical studies on various forms of Pb_2CrO_5 specimens have revealed that most of the physical properties of the fabricated Pb_2CrO_5 devices depend on the conditions of the sample preparation and/or electrode arrangements. So far, thin films of Pb_2CrO_5 have been produced by the electron-beam evaporation (EBE) deposition techniques and were found to give the best electrical performance and possess crystallized structures similar to that of the bulk Pb_2CrO_5 material when prepared at substrate temperatures T_s in the range 100–150 °C and annealed at temperatures between 400 and 500 °C [26, 27].

Regarding the AC behaviour of and photoconduction phenomenon in the Pb_2CrO_5 thin-film devices, not much work has been done and only a few detailed analyses of these electrical properties have been carried out. Moreover, universal values of the relative dielectric constant κ and the room-temperature volume dark resistivity ρ_d of Pb_2CrO_5 have not yet been reported and are not well established. To achieve such a goal we should give

further consideration to the analysis of the electrical and dielectric properties of annealed thin-film devices of this semi-insulating material.

It is the purpose of this study to utilize the above-mentioned types of equivalent-circuit models to discuss and analyse the frequency dependence of the complex-impedance data of a $Au/Pb_2CrO_5/SnO_2$ sandwiched-structure thin-film device prepared under optimum conditions with the device being placed in the dark and in various visible-light environments. The analysis will also be used to deduce representative values for the volume dark resistivity and the relative dielectric constant of the Pb_2CrO_5 material at room temperature.

2. Experimental details

The geometrical details of the $Au/Pb_2CrO_5/SnO_2$ sandwiched-structure thin-film device investigated in this work are shown in figure 1. One side of the Pyrex glass was coated with a Sb-doped SnO_2 transparent film which serves as one electrical electrode for the device. A Pb_2CrO_5 film 0.8 μm thick was deposited on the SnO_2 film at a substrate temperature $T_s = 110\,^{\circ}\mathrm{C}$ by RF magnetron sputtering with a 50 mbar Ar working gas pressure. The RF power for sputtering was 100 W. The distance between the glass substrate and the Pb_2CrO_5 ceramic target used as the source material was 25 mm. After the deposition, the as-deposited

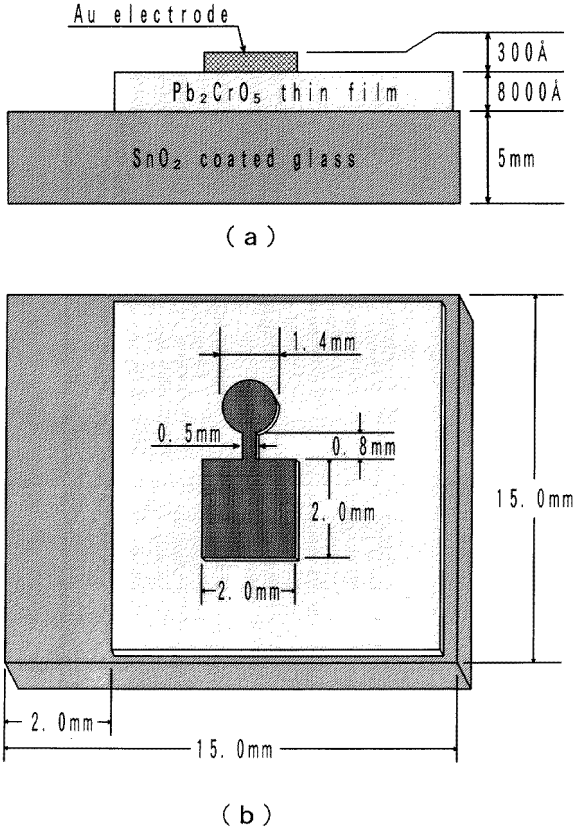

Figure 1. Details of the geometrical structure of the $Au/Pb_2CrO_5/SnO_2$ thin-film device: (a) side view; (b) top view.

film was annealed at $T_a = 450\,^{\circ}$C for 10 h in air to achieve crystallization of the obtained Pb_2CrO_5 film [18–21]. An Au film 30 nm thick was selected to serve as the top electrical electrode.

The crystallization features of the annealed Pb_2CrO_5 thin film have been confirmed by the x-ray diffraction (XRD) patterns of the above-described as-deposited and annealed thin films and these are shown in figure 2. The x-ray source was Cu-Kα radiation at 40 kV and a current of 20 mA. These XRD patterns suggest that the as-deposited film is in the amorphous state, whereas the appearance of the sharp peaks in the case of the annealed Pr_2CrO_5 film is an indication of crystallization of the film as a result of the annealing treatment. Moreover, the XRD pattern of this annealed film is similar to those reported for Pb_2CrO_5 bulk material and similar annealed Pb_2CrO_5 thin films produced by EBE deposition methods [17, 18, 26, 27].

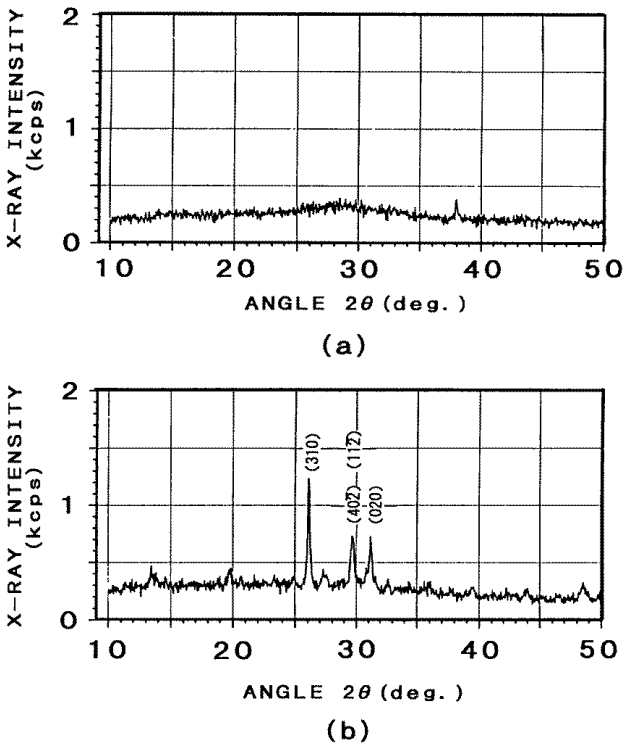

Figure 2. XRD patterns of Pb_2CrO_5 thin films for (a) an as-deposited film at a substrate temperature of 110 °C and (b) a film annealed at 450 °C.

The complex impedance $Z(j\omega)$ of an electrical device at an angular frequency ω of the applied AC signal is expressed as $Z(j\omega) = Z'(\omega) - jZ''(\omega)$, where $Z'(\omega)$ and $Z''(\omega)$ are the real and imaginary parts, respectively, of the complex impedance. In general, AC impedance methods enable one to measure the phase angle $\theta(\omega) = \tan^{-1}\{Z''(\omega)/Z'(\omega)\}$ and the complex-impedance magnitude $|[Z(j\omega)]| = \{[Z'(\omega)]^2 + [Z''(\omega)]^2\}^{1/2}$ of the device under investigation. Two types of experimental arrangement were used to measure these quantities for the Pb_2CrO_5 thin-film device of this work as a function of frequency in the range 0.1 Hz–1.0 MHz and these are represented by the schematic diagrams in figures 3(a) and 3(b). Since the device impedance is high in the low-frequency region, the measuring

circuit in figure 3(a) has been used for the impedance and phase measurements at frequencies between 0.1 Hz and 1 kHz. This experimental set-up incorporates a high-input impedance J-FET operational amplifier (type PMI OP-43EJ), an HP 8165 A oscillator and a digital oscilloscope (LeCroy 9314 L). The uncertainties in the measured values of the complex-impedance magnitude $|[Z(j\omega)]_{meas}|$, and phase angle $[\theta(\omega)]_{meas}$ were better than 3% and 2.5% respectively, at frequencies below 100 Hz but highly improved at higher frequencies. In the frequency range 200 Hz–1.0 MHz, where the device has a low impedance and thus measurements can be carried out using most commercial vector impedance meters, we have used an HP 4192 A impedance analyser to obtain $|[Z(j\omega)]_{meas}|$, and $[\theta(\omega)]_{meas}$ for the device using the set-up in figure 3(b). The results obtained by both methods were in good agreement, within the accuracy of the measurements, for the frequencies between 100 Hz and 1 kHz. The peak-to-peak voltage V_{pp} of the applied AC signal was 2.82 mV, which corresponds to an electric field of 3.525 kV mm^{-1} that is well below the field of instability and/or breakdown in Pb_2CrO_5 thin-film devices [15, 17].

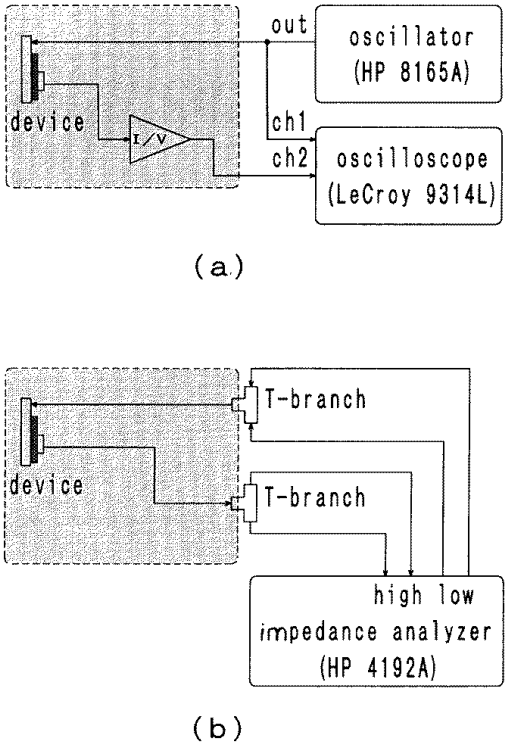

Figure 3. Experimental arrangements for impedance and phase measurements in the frequency ranges (a) 0.1 Hz–1 kHz and (b) 200 Hz–1 MHz.

The measurements of the complex-impedance magnitude and phase angle were carried out at room temperature with the device either being placed under dark conditions or being illuminated with white light produced by a tungsten–halogen lamp (Sylvania JCP; 100 V; 650 W). The maximum photoresponse of Pb_2CrO_5 is often achieved in the visible spectral range between 500 and 600 nm. The light beam was incident and focused upon the upper Au electrode of the device, and the intensity of the falling light was varied and monitored between 0 and 64.8 mW cm^{-2}.

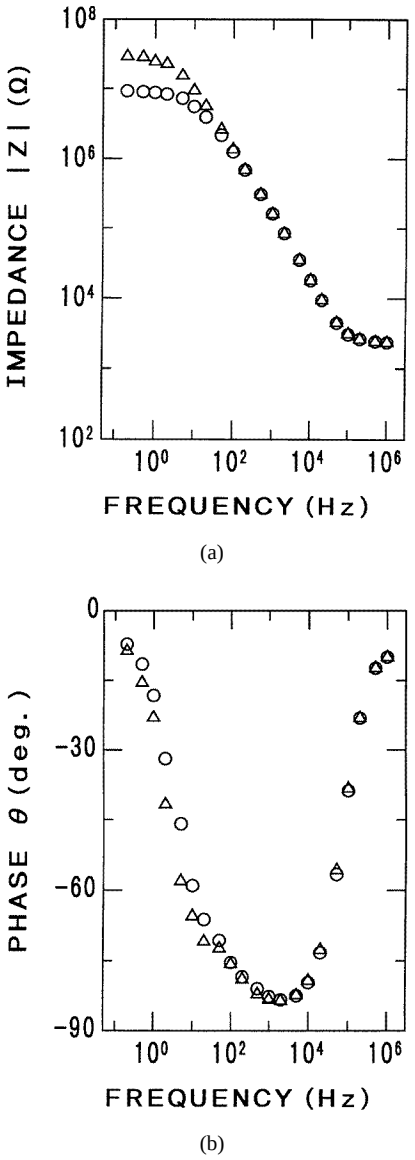

Figure 4. Frequency dependences of (a) the magnitude and (b) the phase of the device impedance: Δ, measured results under dark conditions; O, measured results under a light intensity of 64.8 mW cm^{-2}.

3. Experimental results and discussion

Figures 4(a) and 4(b) show the frequency dependences of the measured complex-impedance magnitude $|[Z(\omega)]_{meas}|$, and phase angle $[\theta(\omega)]_{meas}$ respectively, produced by our Pb_2CrO_5 thin-film device at room temperature under a dark environment and for a light intensity of 64.8 mW cm^{-2}. At high frequency (10^5 Hz or higher), the device impedance is reduced to a low constant value of about 2.5 kΩ, regardless of the intensity of the light illuminating the device. At low frequencies (below 20 Hz), the device impedance tends to saturate

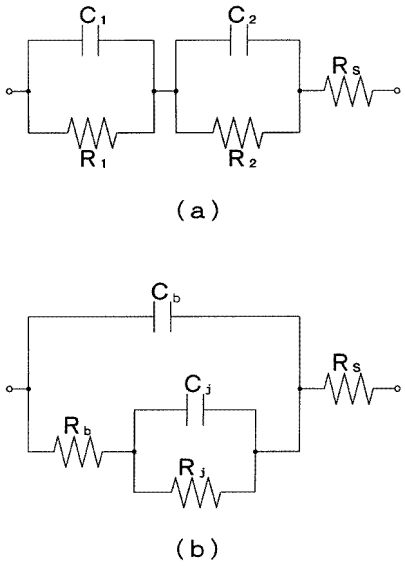

Figure 5. The equivalent circuits used for impedance analysis of the Au/$Pb_2CrO_5SnO_2$ device based on (a) the MW two-layer capacitor model and (b) a model that incorporates the physical meaning of an optoelecronic device.

at a high constant value with $|[Z(\omega)]_{meas}| \simeq 3 \times 10^7\ \Omega$ in the dark case and about $10^7\ \Omega$ when the light intensity was 64.8 mW cm^{-2}. These data suggest that the device is acting as a purely resistive element at the extreme frequencies as can also be seen from the corresponding values of the measured phase angle (i.e. $[\theta(\omega)]_{meas} \rightarrow 0^\circ$). In the intermediate-frequency region, however, the device impedance is a strongly decreasing function of increasing frequency, indicating that the capacitive part of the device becomes more operative. Moreover, the phase angle of the device increases from $[\theta(\omega)]_{meas} = 0^\circ$ at the lowest frequencies towards negative values as the frequency increases and passes through a minimum ($[\theta(\omega)]_{meas} \simeq -90^\circ$) at a frequency of about 4 kHz; after this it starts to rise again towards $[\theta(\omega)]_{meas} = 0^\circ$ with further increase in the frequency.

The overall observed AC behaviour of the Au/Pb_2CrO_5/SnO_2 thin-film device of the present study can be understood if we visualize this device as composed of a Au/Pb_2CrO_5 contact and a bulk Pb_2CrO_5 film whose electrical and dielectric properties are not the same and are dominant in different frequency regions. Such a device can be described by the use of the MW two-layer capacitor model [3–6], in which the permittivity ϵ_1 and electrical resistivity ρ_1 of the metallic–dielectric interface of the device are often represented by a parallel R_1C_1 combination connected in series with another parallel R_2C_2 network for the dielectric bulk material having a different permittivity ϵ_2 and a different electrical resistivity ρ_2. These parallel networks are connected to a series resistance R_s of the film electrodes as depicted in figure 5(a). The complex impedance of this two-layer capacitor system in figure 5(a) can be written as

$$Z_{MW}(\mathrm{j}\omega) = Z'_{MW}(\omega) - \mathrm{j}Z''_{MW}(\omega) \tag{1a}$$

and the corresponding phase angle $[\theta(\omega)]_{MW}$ is given by

$$[\theta(\omega)]_{MW} = \tan^{-1}\{Z''_{MW}(\omega)/Z'_{MW}(\omega)\} \tag{1b}$$

where the real and imaginary parts of $Z_{MW}(\mathrm{j}\omega)$ are expressed as

$$Z'_{MW}(\omega) = R_S + R_1/[1 + (\omega R_1 C_1)^2] + R_2/[1 + (\omega R_2 C_2)^2] \tag{1c}$$

and

$$Z''_{MW}(\omega) = \omega R_1^2 C_1/[1 + (\omega R_1 C_1)^2] + \omega R_2^2 C_2/[1 + (\omega R_2 C_2)^2] \tag{1d}$$

The observed $|[Z(\mathrm{j}\omega)]_{meas}|$–$\omega$ and $[\theta(\omega)]_{meas}$–ω curves can be monitored by the use of the above equations of the MW equivalent-circuit model where the value of $|[Z(\mathrm{j}\omega)]_{meas}|$ becomes independent of frequency ($\sim R_S$) at the high frequencies and saturates at $|[Z(\omega)]_{meas}| \sim R_S + R_1 + R_2$ at the lowest frequencies used. The individual values of the various electrical-circuit parameters of this equivalent circuit have been evaluated over the entire frequency range studied from a thorough fitting analysis of these equations to the measured values of $|[Z(\omega)]_{meas}|$ and $[\theta(\omega)]_{meas}$ for different light intensities. Typical results of the calculated values of these parameters are shown in table 1 and the fitted values of $|Z(\omega)|$ and $\theta(\omega)$ obtained using the MW equivalent-circuit model are represented in figures 6–9 by the solid curves for the dark case and for a light intensity of 64.8 mW cm^{-2}. The experimental results appear to be consistent with the predictions of the MW theory. Furthermore, the electrical and/or dielectric parameters of the investigated Au/Pb_2CrO_5/SnO_2 thin-film device are obviously influenced by the formation of the Au/Pb_2CrO_5 interface and the associated space-charge effects which seem to be enhanced when the device is illuminated with visible light. It can be noted here that the visible light falling on the Au electrode will generate free electrons in the region of the Au film owing to the light absorption as the light energy $h\nu \geqslant \Phi_{BN}$, where $\Phi_{BN} \simeq 2.04$ eV is the barrier height for a Au–Pb_2CrO_5 contact [17]. Moreover, the light transmitted to the Pb_2CrO_5 film will be absorbed near this interface as this light also has an energy $h\nu \geqslant E_g$ and the absorption coefficient of this material is high enough in the visible region of the spectrum. As a result, space-charge effects at such an interface become important. In view of the MW phenomena, this is usually expressed in terms of a frequency-dependent apparent dielectric constant which is always accompanied by large AC losses [3–6].

In order to evaluate the individual electrical, photoelectric and dielectric circuit parameters of the Pb_2CrO_5 bulk-film of the device and its Au–Pb_2CrO_5 interface, we propose a specific equivalent-circuit model, referred to here as the physical model, based on the circuit network shown in figure 5(b), which has been presumed to describe the overall AC behaviour of a practical opto-electronic device. According to this model, the Au–Pb_2CrO_5 contact is represented by a parallel R_jC_j combination in series with the bulk resistance R_b of the Pb_2CrO_5 thin film. This R_jC_j–R_b network is shunted by a parallel capacitance $C_b = \kappa C_0$, where C_0 is the geometrical capacitance of the empty condenser between the Au and SnO_2 electrodes and κ is the relative dielectric constant of the Pb_2CrO_5 bulk film. The whole circuit of the Au–Pb_2CrO_5 interface and the Pb_2CrO_5 film is connected in series with R_S. The complex-impedance magnitude $|Z(\mathrm{j}\omega)|$ and the phase angle $\theta(\omega)$ corresponding to this equivalent-circuit model can be found in terms of $Z'(\omega)$ and $Z''(\omega)$ given by

$$Z'(\omega) = R_S + Z_1(\omega)/Z_2(\omega) \tag{2a}$$

and

$$Z''(\omega) = Z_3(\omega)/Z_2(\omega) \tag{2b}$$

where the functions $Z_1(\omega)$, $Z_2(\omega)$ and $Z_3(\omega)$ are expressed by

$$Z_1(\omega) = R_b(\omega R_j C_j)^2 + (R_b + R_j) \tag{2c}$$

$$Z_2(\omega) = \{1 - [\omega R_j C_j][\omega R_b C_b]\}^2 + [\omega R_j C_j + \omega C_b(R_b + R_j)]^2 \tag{2d}$$

$$Z_3(\omega) = (R_b + R_j)[\omega R_j C_j + \omega C_b(R_b + R_j)] + [(\omega R_b^2 C_b)(\omega R_j C_j)^2 - \omega R_b R_j C_j]. \tag{2e}$$

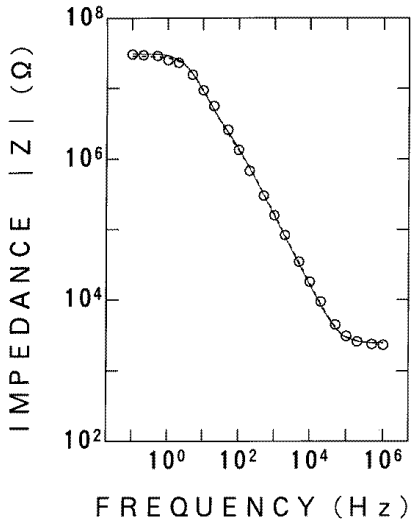

Figure 6. Frequency dependence of the impedance magnitude $|Z(\omega)|$ of the device in the dark: ○, measured data. The calculated values of $|Z(\omega)|$ obtained from the equivalent-circuit models of figure 5(a) (——) and figure 5(b) (- - - -) are also shown.

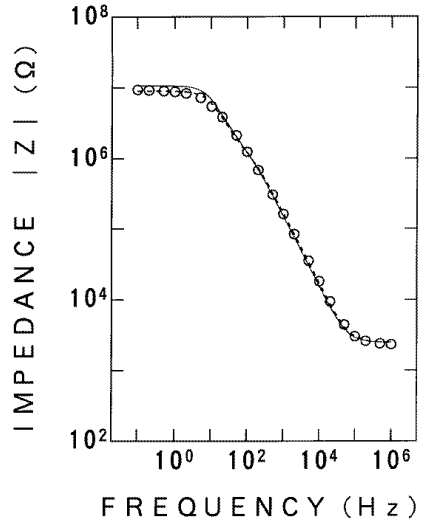

Figure 7. Frequency dependence of the impedance magnitude $|Z(\omega)|$ of the device when illuminated with a light intensity of 64.8 mW cm^{-2}: ○, measured data. The calculated values of $|Z(\omega)|$ obtained from the equivalent-circuit models of figure 5(a) (——) and figure 5(b) (- - - -) are also depicted.

It is obvious that the frequency and/or illumination dependences of $|Z(j\omega)|$ and $\theta(\omega)$ described by equations (2a)–(2e) are too involved but, however, reduce eventually to the appropriate values at the low- and high-frequency extremes. A detailed fitting analysis of the experimental data of the impedance magnitude and phase angle to these equations has been carried out over the entire frequency range for all the illumination levels used in the

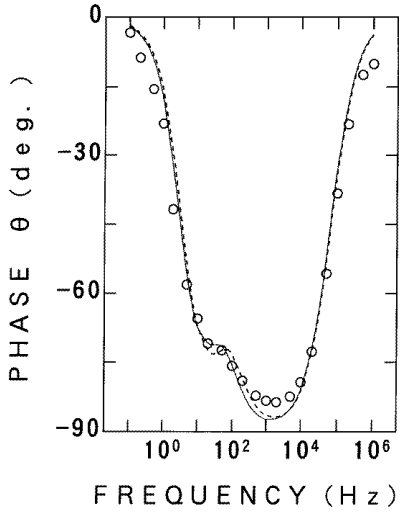

Figure 8. Frequency dependence of the phase angle $\theta(\omega)$ produced by the device in the dark: ○, measured data. The calculated values of $\theta(\omega)$ obtained from the equivalent-circuit models of figure 5(a) (——) and figure 5(b) (- - - -) are also shown.

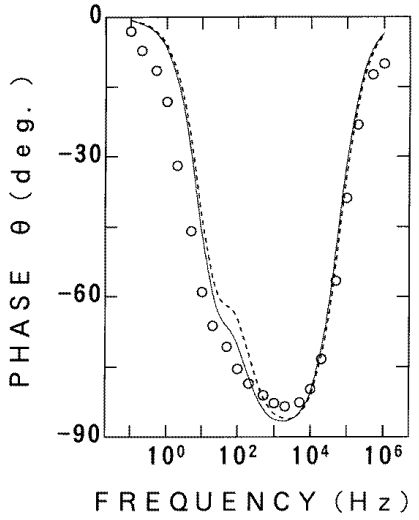

Figure 9. Frequency dependence of the phase angle $\theta(\omega)$ produced by the device when illuminated with a light intensity of 64.8 mW cm^{-2}: ○, measured data. The calculated values of $\theta(\omega)$ obtained from the equivalent-circuit models of figure 5(a) (——) and figure 5(b) (- - - -) are also shown.

study. Some representative results of these calculations are also demonstrated in figures 6–9 as broken curves and summarized in table 2 for the dark case and for an illumination level of 64.8 mW cm^{-2}. The agreement between the experimental data and the fitted results obtained using the proposed physical model of figure 5(b) sounds rather reasonable. It is

also noted from table 2 that the bulk resistance R_b of the Pb_2CrO_5 film decreases when the device is illuminated. The effect of illumination on this resistance is demonstrated in figure 10, where the bulk conductance $G_b = 1/R_b$ has been plotted against the light intensity. Since the Pb_2CrO_5 material belongs to the C2/m space group with a centre of symmetry, these results confirm that the photoconduction phenomenon in Pb_2CrO_5 is due to semiconductivity as a result of the photogeneration of electron–hole pairs in the film of Pb_2CrO_5 upon the absorption of the visible light having energy $h\nu \geqslant E_g$.

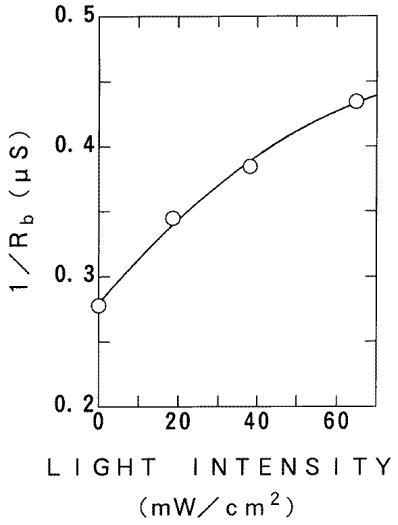

Figure 10. The behaviour of the deduced values of the reciprocal $1/R_b$ of the resistance of the Pb_2CrO_5 film with light intensity: ——, smooth curve through these values.

Using the deduced value of the dark bulk resistance R_b(dark) for the Pb_2CrO_5 film and its dimensions, we have evaluated a value for the room-temperature volume dark resistivity ρ_d for the Pb_2CrO_5 material as $\rho_d \simeq 2.6 \times 10^9$ Ω cm. This value can be categorized to be between the resistivities of semiconductors and dielectrics. On the other hand, the Pb_2CrO_5 film capacitance C_b was found to be independent of the illumination level with a value of about 955 pF. Using this value together with the calculated value of the geometrical capacitance $C_o = 64.05$ pF of the empty condenser, we have determined, for the first time, a value for the relative dielectric constant of Pb_2CrO_5: $\kappa = C_b/C_o \simeq 14.9$. However, both the conductance $G_j(= 1/R_j)$ and the capacitance C_j associated with the Au–Pb_2CrO_5 interface were found to be strongly increasing functions of the intensity of the light illuminating the device as one can see from table 2 and figures 11 and 12, a behaviour attributed to space-charge effects at the interface which appear to be enhanced by illumination.

The actual change in the bulk conductance G_b due to illumination, defined as $\Delta G_b(F) = G_b$(illum)$-G_b$(dark), has been found to vary with the light intensity F as

$$\Delta G_b(F) \propto F^m \tag{3}$$

with $m \simeq 0.7(\pm 5\%)$ and this is demonstrated in figure 13. A similar light intensity dependence of the photoconductance has been observed in several photosensitive electrical devices [15–19, 29, 34–39]. On the other hand, the increase in the interfacial conductance with light intensity, defined as $\Delta G_j(F) = G_j$(illum)$-G_j$(dark), follows equation (3) but

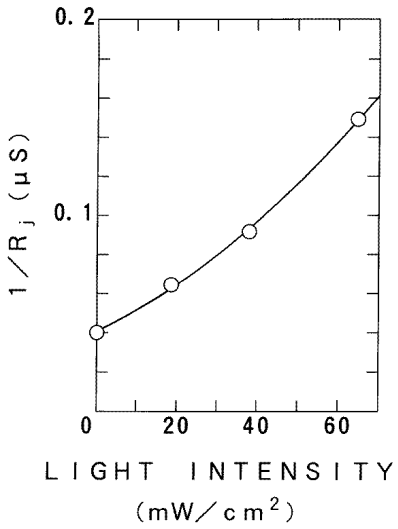

Figure 11. The dependence of the deduced values of the reciprocal $1/R_j$ of the resistance of the Au–Pb_2CrO_5 contact on the light intensity: ——, smooth curve through these values.

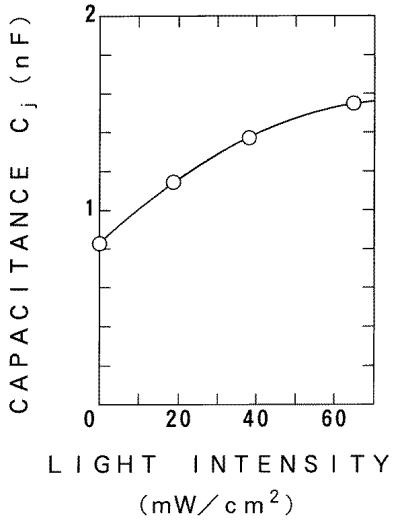

Figure 12. The dependence of the deduced values of the capacitance C_j of the Au–Pb_2CrO_5 contact on light intensity: ——, smooth curve through these values.

with $m \simeq 1.2(\pm 5\%)$ as can be seen from the plot in figure 13. Many theoretical models have been put forward to explain the photoconduction phenomena in dielectric materials [40–50]. In general, most of these models presume that trapping and recombination centres present in a specimen and/or the distribution of the associated energy levels play a major role in the mechanism of its photoconduction but, in principle, the results of such models are too involved. Nevertheless, it is generally accepted that the photoconductivity σ_{phot} can

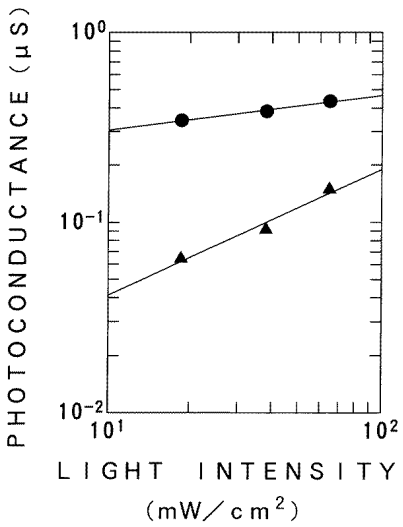

Figure 13. The dependences of the determined values of the photoconductances $\Delta G_b(F) = G_b(\text{illum}) - G_b(\text{dark})$ of the Pb_2CrO_5 film and $\Delta G_j(F) = G_j(\text{illum}) - G_j(\text{dark})$ of the Au–Pb_2CrO_5 contact on the light intensity F: ——, regression fits to the appropriate data; ●, $\Delta G_b(F)$; slope of 0.7; ▲, $\Delta G_j(F)$, slope of 1.2.

be expressed by a power-law dependence on the light intensity of the form

$$\sigma_{phot} \propto F^{\gamma} \tag{4}$$

where the numerical exponent γ is governed by the nature and purity of the specimen under investigation and the strength of the illumination level via the appropriate recombination or generation mechanisms. The observed values of γ often lie in the range 0.5–1.0, although some variations in σ_{phot} with light intensity have been reported to be superlinear (i.e. $\gamma > 1$).

4. Conclusions

A Au/Pb_2CrO_5/SnO_2 sandwiched-structure thin-film device has been produced by the use of RF magnetron sputtering technique and heat treated at a substrate temperature $T_s = 110\,^{\circ}$C and an annealing temperature $T_a = 450\,^{\circ}$C. The device has been investigated from a structural point of view and from the viewpoint of its electrical, photoelectric and dielectric performance as a thin-film photoconducting element. The XRD patterns confirm that the structure of this annealed film specimen involves diffraction peaks similar to those of the bulk material and other thin films produced by the EBE deposition techniques. Impedance measurements on this device in the frequency range 0.1 Hz–1.0 MHz under dark and illumination conditions indicate that the device structure and its electrical and dielectric properties are largely influenced and changed by the formation of the Au–Pb_2CrO_5 contact where interfacial space-charge effects become significant. A thorough analysis of the impedance data by the use of both the MW two-layer capacitor system and an equivalent-circuit model that considers the physical meaning of a practical optical device enables us to determine some new characteristic physical parameters for the Pb_2CrO_5 material such as the volume dark resistivity ρ_d and its relative dielectric constant κ. The deduced

room-temperature values of the dark-resistivity ρ_d and κ were 2.6×10^9 Ω cm and 14.9, respectively. Illumination of the device through the Au-film electrode does not affect the dielectric constant of the Pb_2CrO_5 bulk film while it renders the film material more conductive, a behaviour ascribed to the photogeneration of electron–hole pairs in the bulk of this centrosymmetric dielectric. The bulk photoconductance of the film has been found to vary with light intensity F as $\Delta G_b(F) \propto F^{0.7}$, in good agreement with theoretical predictions and other observations in many dielectric solids. On the other hand, electrode and interfacial space-charge polarization effects were found to be important and sometimes strongly influence the electrical performance of the device. These effects often manifest themselves in the behaviour of the associated electrical parameters with frequency and/or illumination, which seems to enhance them.

References

[1] Welsh H K 1985 *J. Phys. C: Solid State Phys.* **18** 5641
[2] Dyre J C 1991 *J. Non-Cryst. Solids* **135** 219
[3] Goto Y 1981 *J. Phys. Soc. Japan* **50** 538, 1241
[4] Rapsos M and Calderwood J H 1978 *Proc. Conf. on Dielectric Materials, Measurements and Applications (IEE Conf. Publ. 125)* (London: IEE) p 162
Rapsos M and Calderwood J H 1979 *Proc. Conf. on Dielectric Materials, Measurements and Applications (IEE Conf. Publ. 177)* (London: IEE) p 306
[5] Hill N E, Vaughan W E, Price A H and Davies M 1969 *Dielectric Properties and Molecular Behavior* 1st edn (London: Van Nostrand Reinhold)
[6] Kittel C 1996 *Introduction to Solid State Physics* 7th edn (Chichester: Wiley)
[7] Antohe S 1993 *Phys. Status Solidi* a **136** 401
[8] Shur M 1990 *Physics of Semiconductor Devices* (Englewood Cliffs, NJ: Prentice-Hall)
[9] Sze S M 1981 *Physics of Semiconductor Devices* 2nd edn (New York: Wiley)
Sze S M 1985 *Semiconductor Devices: Physics and Technology* (New York: Wiley)
[10] Ahmad-Bitar R N, Abdul-Gader M M, Wishah K A, Mahmud Y A and Hassan M H 1984 *Nucl. Instrum. Methods* A **243** 505
Ahmad-Bitar R N, Khomayes S J, Wishah K A, Abdul-Gader M M and Mahmud Y A 1994 *Dirasat (Pure Appl. Sci.)* B **21** 41
[11] Jonscher A J 1983 *Dielectric Relaxation in Solids* (London: Chelsea College Press)
Jonscher A J 1991 *J. Mater Sci.* **26** 1618
[12] Regolini J L and Saura J 1983 *J. Appl. Phys.* **54** 1528
[13] Simmons J G, Nadkarni G S and Lancaster M C 1970 *J. Appl. Phys.* **41** 538
Nadkarni G S and Simmons J G 1970 *J. Appl. Phys.* **41** 545
Simmons J G 1970 *Hand Book of Thin Film Technology* ed L I Maissel and R Glang (New York: McGraw-Hill)
[14] Doi A 1989 *J. Mater. Sci.* **24** 749
[15] Yoshida S and Toda K 1990 *Appl. Optics* **29** 1793
[16] Toda K and Yoshida S 1988 *J. Appl. Phys.* **63** 1580
[17] Toda K and Yoshida S 1989 *Appl. Phys.* **65** 857
[18] Toda K, Yoshida S and Ikenaga H 1993 *J. Mater. Sci. Lett.* **12** 478
[19] Toda K and Shingo Watanabe 1995 *J. Appl. Phys.* **77** 2786
[20] Mostafa M F, Abdel-Kader M M, Atallah A S and El-Nimer M 1993 *Phys. Status Solidi* a **135** 549
[21] Jae-Hyung Kim, Jeong-Bae Kim, Kwang-Sei Lee, Byung-Chum Choi, Jung-Nam Kim and Su-Dae Lee 1993 *Solid State Commun.* **86** 257
[22] Saleh A M, Gould R D and Hassan A K 1993 *Phys. Status Solidi* a **139** 379
[23] Wiktorczyk T 1993 *Phys. Status Solidi* a **139** 397
[24] Diallo A T and Arof A K 1993 *Jur. Sains.* **1** 30
[25] Macdonald J R 1987 *Impedance Spectroscopy* (New York: Wiley)
[26] Morita S and Toda K 1985 *Appl. Phys.* A **36** 131
[27] Toda K and Morita S 1985 *J. Appl. Phys.* **57** 5325
[28] Toda K and Morita S 1984 *J. Appl. Phys.* **55** 210
[29] Toda K and Morita S 1984 *Appl. Phys.* A **33** 231

[30] Morita S and Toda K 1984 *J. Appl. Phys.* **55** 2733
[31] Abdul-Gader M M, Wishah K A, Mahmud Y A, Toda K and Ahmad-Bitar R N 1989 *Appl. Phys.* A **49** 665
[32] Negas T 1968 *J. Am. Ceram. Soc.* **51** 716
[33] Ruckman J C, Morrison R T W and Buck R H 1972 *J. Chem. Soc., Dalton Trans.* 426
[34] Carles D, Vautier C and Viger C 1973 *Thin Solid Films* **17** 67
Grenet J, Carels D, Lefrancois G and Larmagnac J P 1983 *J. Non-Cryst. Solids* **56** 285
[35] Carles D, Lefrancois G and Larmagnac J P 1984 *J. Physique Lett.* **45** L 901
[36] El-Halawany S, Bacewiz R, Filipowicz J and Trykozko R 1984 *Phys. Status Solidi* a **84** K 89
[37] Ozdemir S and Oktu O 1989 *J. Non-Cryst. Solids* **107** 289
[38] Shukla R, Khurana P and Srivastava K K 1991 *Phil. Mag.* B **64** 389
[39] El Charras Z, Bourahla B and Vautier C 1993 *J. Non-Cryst. Solids* **155** 171
Kotkata M F, Fustoss-Wegner M, Toth L, Zentai G and Nouh S A 1993 *J. Phys. D: Appl. Phys.* **26** 456
[40] Hack M, Guha S and Shur M 1984 *Phys. Rev.* B **30** 6991
[41] Bube R H 1960 *Photoconductivity in Solids* (New York: Wiley)
[42] Rose A 1963 *Photoconductivity and Related Processes* (New York: Interscience)
[43] Pyvkin S M 1964 *Photoelectric Effects in Semiconductors* (New York: Consultants Bureau)
[44] Gorlich P 1967 *Photoconductivity in Solids* (New York: Dover)
[45] Mort J and Pai D M (ed) 1976 *Photoconductivity and Related Phenomena* (Amsterdam: Elsevier)
[46] Kittel C 1971 *Introduction to Solid State Physics* 4th edn (Chichester: Wiley)
[47] Mott N F and Davies E A 1979 *Electronic Processes in Non-Crystalline Materials* (Oxford: Clarendon)
[48] Kireev P S 1975 *Semiconductor Physics* (Moscow: Mir)
[49] Hava S 1986 *J. Appl. Phys.* **59** 4097
[50] Halpern V 1988 *J. Phys. C: Solid State Phys.* **21** 2555